

Supporting Information

Woodhouse and Goldstein 10.1073/pnas.1302736110

SI Text

This document is organized as follows. We first present a derivation of the model dynamics from the full Smoluchowski equation and nondimensionalization of all parameters. Following this, we give a linear stability analysis and the subsequent reasoning for the selected filament-forcing relationship. We then investigate the intricate pattern-forming dynamics of the model by studying the reduced z -independent system. Finally, we briefly discuss interpretations of streaming pathologies within this model.

Model

Geometry. The *Chara* cell cytoplasm is modeled as a cylindrical shell of radius R and length L , endowed with periodic boundary conditions for all fields unless otherwise noted. The shell is parameterized with standard cylindrical coordinates (θ, z) , with $\theta \in [0, 2\pi)$ and $z \in [0, L)$. On a cylindrical shell, the gradient operator reads

$$\nabla = \mathbf{e}_\theta \frac{1}{R} \frac{\partial}{\partial \theta} + \mathbf{e}_z \frac{\partial}{\partial z},$$

and so the Laplacian is equivalent to the Cartesian Laplacian with a spatial scaling by R . After nondimensionalization of space by R , this factor will disappear and the gradient operator becomes identical to Cartesian space.

Smoluchowski Equation and Derivation. To derive the actin filament suspension dynamics, we begin by writing down a Smoluchowski equation for the spatial and orientational filament density $(1, 2)$. At every point $\mathbf{x} = (\theta, z)$ on the cylinder, let $\Psi(\mathbf{x}, \mathbf{p})$ be the number density at position \mathbf{x} of filaments with orientation \mathbf{p} , $|\mathbf{p}| = 1$, where \mathbf{p} points from the minus (pointed) end to the plus (barbed) end. From this, we define the orientational averaging operator:

$$\langle \cdot \rangle = \int_{\mathbf{p}} \cdot d\mathbf{p}.$$

Then the filament concentration $c(\mathbf{x})$ and polar moment $\mathbf{P}(\mathbf{x})$ are given by the following:

$$c = \langle 1 \rangle, \\ c\mathbf{P} = \langle \mathbf{p} \rangle.$$

Now, suppose further that the filaments are suspended in a fluid with associated flow field $\mathbf{u}(\mathbf{x})$. The Smoluchowski equation reads

$$\frac{\partial \Psi}{\partial t} = -\nabla_x \cdot (\dot{\mathbf{x}} \Psi) - \nabla_p \cdot (\dot{\mathbf{p}} \Psi), \quad [\text{S1}]$$

where $\nabla_x = \partial/\partial \mathbf{x}$, and $\nabla_p = (\mathbb{I} - \mathbf{p}\mathbf{p}) \cdot \partial/\partial \mathbf{p}$ is the gradient operator on the unit circle. The one-filament velocity is the following:

$$\dot{\mathbf{x}} = \epsilon \mathbf{u} + w \mathbf{p} - D^{(s)} \nabla_x \log \Psi,$$

where ϵ is the effectiveness of flow-advection (restriction), w is the advection velocity of a filament by a myosin (self-advection), and $D^{(s)}$ is the spatial diffusion constant. (Note $w < 0$; filaments will be advected backward relative to the walk direction of the myosin motors.) The one-filament orientational change schematically reads

$$\dot{\mathbf{p}} = (\mathbb{I} - \mathbf{p}\mathbf{p}) \cdot (\text{shear alignment} + \text{flow alignment} + \text{directional bias} + \text{polarization} + \text{diffusion}).$$

The terms are as follows:

$$\begin{aligned} \text{shear alignment} &= \epsilon \Omega \cdot \mathbf{p} \\ \text{flow alignment} &= \alpha_u \mathbf{u} \\ \text{directional bias} &= -\kappa (\mathbf{P} \cdot \mathbf{d}) \mathbf{d} \\ \text{polarization} &= \alpha_p \mathbf{P} \\ \text{diffusion} &= -D^{(r)} \nabla_p \log \Psi, \end{aligned}$$

with α_p, α_u , the coupling constants for spontaneous polarization and polar flow alignment, respectively; κ , the coupling for directional bias away from orientation in the \mathbf{d} -direction; and $D^{(r)}$, the rotational diffusion constant. Ω is the Jeffery tensor, where $\Omega = \nabla \mathbf{u}$ for rodlike particles (3).

Taking the orientational average of Eq. S1 yields c dynamics reading

$$\frac{\partial c}{\partial t} + \nabla \cdot [(\epsilon \mathbf{u} + w \mathbf{P}) c] = D^{(s)} \nabla^2 c.$$

Multiplying Eq. S1 by \mathbf{p} and taking the orientational average gives dynamics of $c\mathbf{P}$. Inserting the above c dynamics then yields final \mathbf{P} dynamics of

$$\begin{aligned} \frac{\partial \mathbf{P}}{\partial t} + (\epsilon \mathbf{u} + w \mathbf{P}) \cdot \nabla \mathbf{P} &= D^{(s)} \left(\nabla^2 \mathbf{P} + \frac{2}{c} \nabla c \cdot \nabla \mathbf{P} \right) - D^{(r)} \mathbf{P} \\ &+ (\mathbb{I} - \mathbf{p}\mathbf{p}) \cdot [\epsilon \Omega \cdot \mathbf{P} + \alpha_p \mathbf{P} + \alpha_u \mathbf{u} - \kappa (\mathbf{P} \cdot \mathbf{d}) \mathbf{d}], \end{aligned}$$

after applying the elementary Doi-like (4) closures $\langle \mathbf{p}\mathbf{p} \rangle \simeq c\mathbf{P}\mathbf{P}$ and $\langle \mathbf{p}\mathbf{p}\mathbf{p} \rangle \simeq c\mathbf{P}\mathbf{P}\mathbf{P}$.

Flow Field. To close the system, we must define the hydrodynamics of the flow field $\mathbf{u}(\mathbf{x})$. Owing to the low velocities and length scales involved, we take \mathbf{u} to obey the 2D incompressible Stokes equations with friction and forcing terms, viz.,

$$-\mu \nabla^2 \mathbf{u} + \nu \mathbf{u} + \nabla \Pi = \mathbf{F}, \quad \nabla \cdot \mathbf{u} = 0,$$

where μ is the viscosity, ν is the friction coefficient, $\Pi(\mathbf{x})$ is the pressure field, and $\mathbf{F}(\mathbf{x})$ is the flow forcing. Incompressibility and friction are consequences of the inner and outer radial boundaries sandwiching the layer of cytoplasm and arise on radial averaging, as we will now discuss.

The incompressibility arises from the proximity of the vacuolar membrane to the cytoplasm. Certainly the cytoplasm is three-dimensionally incompressible, but on radial averaging it need not automatically become two-dimensionally incompressible. However, the vacuolar membrane adjacent to the cytoplasm is a lipid bilayer, which behaves as a true two-dimensionally incompressible fluid (5). A no-slip boundary condition between the cytoplasm and membrane therefore implies that the radially averaged cytoplasm remains approximately incompressible.

The friction term can be viewed as the effect of the other radial boundary on the cytoplasmic layer, the chloroplast/cortical layer to which the filaments adhere. This acts as an outer no-slip boundary yielding a local shear flow profile radially. Upon depth averaging, this becomes a friction term, similar to flow in a Hele-Shaw cell (6).

Finally, we impose a further condition on the flow field to mimic the effects of the flux-limiting end caps of a cell. To this end, we prescribe the zero-flux condition:

$$\int_0^{2\pi} \int_0^L \mathbf{u} \cdot \mathbf{e}_z \, dz d\theta = 0.$$

This prevents a net axial flow that would be impossible in a capped cell owing to the cytoplasm incompressibility. However, to support such a condition we require an additional degree of freedom, which we insert into the pressure field $\Pi(\mathbf{x})$ by allowing a non-periodic linear pressure gradient:

$$\Pi(\mathbf{x}) = \Pi_0 z + \Pi'(\mathbf{x}),$$

where $\Pi'(\mathbf{x})$ is a periodic pressure field supporting incompressibility. Π_0 then acts to support any net upward forcing.

To completely close the system, we must specify the forcing \mathbf{F} in terms of the filament field \mathbf{P} . Naively, one might take $\mathbf{F} \propto \mathbf{P}$; however, this is unsuitable for our model. We postpone the reasoning until the linear stability analysis and simply state here that we will take $\mathbf{F} = \Phi |\mathbf{P}|^2 \mathbf{P}$, where Φ is a force proportionality constant.

Nondimensionalization. Define the total filament number

$$\int_A c \, dA = c_0 |A|$$

over the cylinder surface A with area $|A|$, so c_0 is the mean filament concentration. We choose a friction-based timescale

$$\tau \equiv \frac{c_0}{\nu}.$$

We choose to scale all lengths by the cylinder radius R . Then using c_0, τ, R , we can nondimensionalize all parameters and variables as follows. Variables scale as follows:

$$\begin{aligned} \mathbf{x} &= R \hat{\mathbf{x}} \\ t &= \tau \hat{t} \\ \mathbf{u} &= R \tau^{-1} \hat{\mathbf{u}} = R \nu c_0^{-1} \hat{\mathbf{u}} \\ c &= c_0 \hat{c} \\ \Pi &= \nu^2 R^2 c_0^{-1} \hat{\Pi}. \end{aligned}$$

Parameters scale as follows:

$$\begin{aligned} L &= R \ell \\ \mu &= \nu R^2 \hat{\mu} \\ \Phi &= \nu^2 R c_0^{-1} \hat{\Phi} \\ w &= R \tau^{-1} \hat{w} = R \nu c_0^{-1} \hat{w} \\ D^{(s)} &= R^2 \tau^{-1} d^{(s)} = \nu R^2 c_0^{-1} d^{(s)} \\ D^{(r)} &= \tau^{-1} d^{(r)} = \nu c_0^{-1} d^{(r)} \\ \alpha_u &= R^{-1} \hat{\alpha}_u \\ \alpha_p &= \nu c_0^{-1} \hat{\alpha}_p \\ \kappa &= \nu c_0^{-1} \hat{\kappa}. \end{aligned}$$

This eliminates ν in the nondimensional system. We can eliminate $\hat{\Phi}$ by further rescaling as follows:

$$\begin{aligned} \hat{\mathbf{u}} &= \hat{\Phi} \hat{\hat{\mathbf{u}}} \\ \hat{\Pi} &= \hat{\Phi} \hat{\hat{\Pi}} \\ \hat{\epsilon} &= \hat{\Phi}^{-1} \hat{\hat{\epsilon}} \\ \hat{\alpha}_u &= \hat{\Phi}^{-1} \hat{\hat{\alpha}}_u. \end{aligned}$$

Under the above scalings, ν, Φ, R, c_0 are eliminated. Note also that the cylinder now has nondimensional length ℓ .

Zero-Walk Approximation. If we assume that friction is high enough such that a filament can be considered stationary when a myosin-coated vesicle walks along it, then we can take $w = 0$. This important simplification reduces the c dynamics to pure incompressible advection–diffusion, which allows us to then neglect concentration fluctuations. Under this approximation and in nondimensional variables (with all hats on variables now removed), the final system reads

$$-\mu \nabla^2 \mathbf{u} + \mathbf{u} + \Pi_0 \mathbf{e}_z + \nabla \Pi' = |\mathbf{P}|^2 \mathbf{P},$$

subject to

$$\nabla \cdot \mathbf{u} = 0, \quad \int_0^{2\pi} \int_0^\ell \mathbf{u} \cdot \mathbf{e}_z \, dz \, d\theta = 0,$$

with

$$\begin{aligned} \frac{\partial \mathbf{P}}{\partial t} + \epsilon \mathbf{u} \cdot \nabla \mathbf{P} &= d^{(s)} \nabla^2 \mathbf{P} - d^{(r)} \mathbf{P} + (\mathbb{I} - \mathbf{P}\mathbf{P}) \cdot [\epsilon \Omega \cdot \mathbf{P} \\ &+ \alpha_u \mathbf{u} + \alpha_p \mathbf{P} - \kappa (\mathbf{P} \cdot \mathbf{d}) \mathbf{d}]. \end{aligned}$$

In what follows we set the repulsive direction $\mathbf{d} = \mathbf{e}_\theta$.

Linear Stability and Flow Forcing. To determine linear stability of the disordered state $\mathbf{P} = 0$, write $\mathbf{P} = \eta \tilde{\mathbf{P}} + O(\eta^2)$, $\eta \ll 1$ and $\mathbf{u} = \eta \tilde{\mathbf{u}} + O(\eta^2)$. Then to $O(\eta)$, the dynamics read

$$\frac{\partial \tilde{\mathbf{P}}}{\partial t} = d^{(s)} \nabla^2 \tilde{\mathbf{P}} - d^{(r)} \tilde{\mathbf{P}} + \alpha_u \tilde{\mathbf{u}} + \alpha_p \tilde{\mathbf{P}} - \kappa (\tilde{\mathbf{P}} \cdot \mathbf{e}_\theta) \mathbf{e}_\theta.$$

If $\tilde{\mathbf{u}} \sim \tilde{\mathbf{P}}$, then myosin-generated flow alone will drive instability. However, when a totally disordered filament configuration has been created experimentally, vesicles can still be observed to walk along filaments without any global regeneration of ordered streaming (7). Therefore, it is important that this α_u term does not contribute to spontaneous organization, and so we must have $\tilde{\mathbf{u}}$ of higher order than η . This corresponds to a higher-order flow forcing \mathbf{F} , so we take the force field to be $\mathbf{F} = |\mathbf{P}|^2 \mathbf{P}$, as stated previously, which yields $\tilde{\mathbf{u}} = 0$ as desired.

Now, write $\tilde{\mathbf{P}} = \hat{\mathbf{P}} e^{st + ik \cdot \mathbf{x}}$. Then

$$s \hat{\mathbf{P}} = -d^{(s)} |\mathbf{k}|^2 \hat{\mathbf{P}} - d^{(r)} \hat{\mathbf{P}} + \alpha_p \hat{\mathbf{P}} - \kappa (\hat{\mathbf{P}} \cdot \mathbf{e}_\theta) \mathbf{e}_\theta.$$

Eigenvectors are \mathbf{e}_θ and \mathbf{e}_z , with eigenvalues

$$\begin{aligned} s_\theta &= -d^{(s)} |\mathbf{k}|^2 - d^{(r)} - \kappa + \alpha_p, \\ s_z &= -d^{(s)} |\mathbf{k}|^2 - d^{(r)} + \alpha_p. \end{aligned}$$

Therefore, if $\alpha_p > d^{(r)}$, then at least one mode is unstable.

Note that periodicity imposes the quantization $\mathbf{k} = n \mathbf{e}_\theta + (2\pi/\ell) m \mathbf{e}_z$, $n, m \in \mathbb{Z}$.

A Side Note on Closure. Earlier, we used the simple moment closures $\langle \mathbf{p}\mathbf{p} \rangle \simeq c \mathbf{P}\mathbf{P}$ and $\langle \mathbf{p}\mathbf{p}\mathbf{p} \rangle \simeq c \mathbf{P}\mathbf{P}\mathbf{P}$. This is a very strong reduction, similar in character to that of Doi (4) who closed the fourth moment of a nematic distribution as the product of its two second moments. However, these approximations are inaccurate in two key manners: they do not satisfy elementary index-contraction identities, i.e., $\langle p_i p_i \rangle = c$ and $\langle p_i p_j p_j \rangle = c P_i$, and the second-moment closure is not correct in the limit of isotropy,

where $\mathbf{P}=0$ and $\langle \mathbf{p}\mathbf{p} \rangle_{\text{iso}} = \mathbb{I}/2$. More precise closures built on the first moment \mathbf{P} that obey both of these criteria are as follows:

$$\begin{aligned} \langle p_i p_j \rangle &\simeq c P_i P_j + (c/2)(1 - P^2) \delta_{ij}, \\ \langle p_i p_j p_k \rangle &\simeq c P_i P_j P_k + (c/4)(1 - P^2) (\delta_{ij} P_k + \delta_{jk} P_i + \delta_{ki} P_j). \end{aligned}$$

These can be viewed as interpolations between closures accurate in the limits of isotropy and perfect alignment. The derivation above can then be performed with these more complicated expressions. This yields a dynamical system with far more nonlinear terms; however, these are all of the same order, and we expect no qualitative difference from the simpler closure we chose above. The other change of note is in the coefficients of the terms linear in $\alpha_p \mathbf{P}$ and $\alpha_u \mathbf{u}$, which gain a factor of 1/2; this lowers the threshold for spontaneous streaming emergence. Again, though, this is a purely quantitative change. Given this, we believe that using the simpler closure does not obscure the essential dynamics and leads to a cleaner, more manageable system.

In fact, one does not need to make a closure at all to observe the initial instability of the homogeneous, isotropic configuration; this is the method used by Saintillan and Shelley (1) to derive instability of dilute microswimmer suspensions. Starting with the Smoluchowski Eq. S1 after nondimensionalization and the zero-walk approximation, we linearize about the isotropic state $\Psi \equiv 1/2\pi$ by letting

$$\Psi = \frac{1}{2\pi} (1 + \eta \Psi'), \quad \eta \ll 1.$$

With the nonlinear forcing used above, all hydrodynamic fields are of high order, i.e., $\mathbf{u}, \Omega = O(\eta^3)$, so terms involving them can be neglected, as designed. Then after some calculus we obtain

$$\frac{\partial \Psi'}{\partial t} = d^{(s)} \nabla_x^2 \Psi' + d^{(r)} \nabla_p^2 \Psi' + \alpha_p \mathbf{P} \cdot \mathbf{P}' - \kappa (\mathbf{p} \cdot \mathbf{d}) (\mathbf{P}' \cdot \mathbf{d}),$$

where $\mathbf{P}' \equiv \int_p \Psi' \mathbf{p} d\mathbf{p}$ is the perturbation polar order field. The linear term $\alpha_p \mathbf{P} \cdot \mathbf{P}'$ acts to drive spontaneous polarity, reinforcing the mean polar order \mathbf{P}' , which competes with diffusion and directionality. Thus, for sufficiently large α_p , there will be an instability of the isotropic state into local spontaneous polar ordering. It is in this regime that closure systems then become appropriate for understanding the nonlinear, long-time dynamics.

Reduced z-independent System. To get a flavor of the more delicate properties the model possesses from a dynamical systems point of view, we will reduce to the z-independent and \mathbf{e}_z -parallel case. Under this approximation, writing $\mathbf{P} = P \mathbf{e}_z$ and $\mathbf{u} = u \mathbf{e}_z$, the model reduces to

$$\frac{\partial P}{\partial t} = d^{(s)} \frac{\partial^2 P}{\partial \theta^2} - d^{(r)} P + (1 - P^2) (\alpha_p P + \alpha_u u) \quad [\text{S2}]$$

subject to hydrodynamics

$$-\mu \frac{\partial^2 u}{\partial \theta^2} + u = P^3 - \frac{1}{2\pi} \int_0^{2\pi} P(\theta')^3 d\theta',$$

where the pressure gradient Π_0 has been solved for by using the zero-flux condition $\int_0^{2\pi} u d\theta = 0$.

Define a cyclosis solution $P_C(\theta)$ to be a steady-state configuration possessing two antiparallel regions of equal width. We are interested in two questions: are such states stable, and if they are, can the system reach such a state from given initial conditions?

Cyclosis Instability When $\alpha_u = 0$. When $\alpha_u = 0$, the hydrodynamics drop out entirely and Eq. S2 reduces to

$$\frac{\partial P}{\partial t} = d^{(s)} \frac{\partial^2 P}{\partial \theta^2} - d^{(r)} P + \alpha_p (1 - P^2) P. \quad [\text{S3}]$$

This is the one-dimensional Allen–Cahn equation (or Chafee–Infante equation) describing evolution of a nonconserved order parameter P in a symmetric bistable potential $V(P)$ satisfying $V'(P) = d^{(r)} P - \alpha_p (1 - P^2) P$. The state $P=0$ is an unstable equilibrium, so for sufficiently small $d^{(s)}$ the system forms patterns of values $\pm P_*$, where $V'(\pm P_*) = 0$.

A cyclosis perturbation $P(\theta, t) = P_C(\theta) + \eta e^{\lambda t} \phi(\theta)$, $\eta \ll 1$, generates a Sturm–Liouville problem for the growth rate λ reading

$$\lambda \phi = d^{(s)} \phi'' - V''(P_C) \phi. \quad [\text{S4}]$$

Ref. 8 then argues that there always exists an unstable mode, i.e., one with $\lambda > 0$, as follows. Fundamental Sturm–Liouville theory tells us that there exists a discrete spectrum of eigenvalues $\{\lambda_n\}$ satisfying $\lambda_0 > \lambda_1 > \lambda_2 > \dots > -\infty$, and that the eigenfunction ϕ_n corresponding to eigenvalue λ_n changes sign precisely n times within $[0, 2\pi)$. Now, by differentiating Eq. S3, one can see that $\phi = P_C'$ is an eigenfunction of Eq. S4 with $\lambda = 0$. However, by definition P_C crosses the axis twice, so P_C' crosses the axis once, i.e., $\phi_1 \propto P_C'$ and so $\lambda_1 = 0$. Therefore, $\lambda_0 > \lambda_1 = 0$ by the ordering property, rendering the cyclosis solution unstable.

As an aside, we note that, although the cyclosis solution is unstable, the instability (which manifests as attraction and coalescence of the “fronts” between the $\pm P_*$ regions) operates on an extremely long timescale (8).

Cyclosis Stability When $\alpha_u \geq 0$. When $\alpha_u \neq 0$, we must include the effects of hydrodynamics on steady-state stability. Intuitively, one expects the hydrodynamics to stabilize the front coalescence and so render cyclosis stable, at least above some threshold value of α_u . This is indeed what occurs, with a remarkably small threshold, as we will now discuss. To make progress and to simplify matters, we will take $\mu = 0$ to reduce the hydrodynamics to

$$u = P^3 - \frac{1}{2\pi} \int_0^{2\pi} P(\theta')^3 d\theta'.$$

We can then substitute the hydrodynamics directly into Eq. S2 to obtain the following:

$$\begin{aligned} \frac{\partial P}{\partial t} = d^{(s)} \frac{\partial^2 P}{\partial \theta^2} - d^{(r)} P + \alpha_p (1 - P^2) P \\ + \alpha_u (1 - P^2) \left(P^3 - \frac{1}{2\pi} \int_0^{2\pi} P(\theta', t)^3 d\theta' \right). \end{aligned} \quad [\text{S5}]$$

Performing the same perturbation to a cyclosis steady-state P_C of Eq. S5 as above yields a more general “nonlocal” eigenvalue problem:

$$\lambda \phi = d^{(s)} \phi'' - W''(P_C) \phi - \frac{\alpha_u}{2\pi} (1 - P_C^2) \int_0^{2\pi} 3P_C(\theta')^2 \phi(\theta') d\theta', \quad [\text{S6}]$$

where the potential $W(P)$ satisfies $W'(P) = d^{(r)} P - \alpha_p (1 - P^2) P - \alpha_u (1 - P^2) P^3$. In the absence of the integral term, we could make similar arguments as above and derive instability; here,

however, the Sturm–Liouville theory does not apply, so we must work harder and explicitly determine the eigenvalue spectrum.

In general, less is known about such nonlocal systems, but progress is still possible. Ref. 9 demonstrates that the nonlocal problem is intimately linked to the corresponding local problem,

$$\nu\psi = d^{(s)}\psi'' - W''(P_C)\psi,$$

in the following way: if ψ_n is an eigenfunction of the nonlocal problem, with eigenvalue ν_n , then $\phi = \psi_n$ is an eigenfunction with eigenvalue $\lambda = \nu_n$ if $\int 3P_0^2\psi_n = 0$. Therefore, by symmetry arguments, we at least retain the odd eigenfunctions $\phi_{2n+1} = \psi_{2n+1}$ with eigenvalues $\lambda_{2n+1} = \nu_{2n+1}$. In particular, we retain the eigenvalue $\lambda_1 = \nu_1 = 0$, the translational mode with eigenfunction $\phi_1 \propto P_C$ as discussed above for the case $\alpha_u = 0$.

It remains to determine whether there exist any positive eigenvalues. At this stage, little further progress can be made analytically as our system is not self-adjoint (9), so we study the largest eigenvalues numerically. The base cyclosis state P_C is determined by seeding initial conditions purely in the $k=1$ wavenumber and evolving this through time until steady state is reached. A truncated Fourier expansion for ϕ is then used, reducing the problem to determining eigenvalues of a matrix. If α_u is then varied while all parameters are held fixed, an eigenvalue “trajectory” can be plotted; example trajectories for the largest two eigenvalues for one particular parameter set are shown in Fig. S1A. Finally, by interpolating to extract the crossover point of these maximal eigenvalues, a critical value of α_u can be determined where the cyclosis state switches stability, being stabilized for larger α_u owing to flow effects.

Fig. S1B illustrates this critical boundary in the (α_p, α_u) plane with other parameters held fixed as in Figs. 4 and 5. The critical values of α_u quickly become negligible as α_p increases, demonstrating the powerful stabilizing effect of the flow reorientation.

Unidirectional Stability. We now consider the stability of the unidirectional nonflowing solution $P(\theta) \equiv P_*$. By Eq. S2, this satisfies

$$P_*^2 = 1 - \frac{d^{(r)}}{\alpha_p},$$

so a constant solution only exists when $\alpha_p > d^{(r)}$, i.e., when the zero-state $P=0$ is unstable. In the same manner as for the cyclosis solutions, we perturb about this state by writing $P = P_* + \eta e^{i\theta}\phi(\theta)$, $\eta \ll 1$. Then ϕ satisfies

$$\begin{aligned} \lambda\phi = & d^{(s)}\phi'' - \left(W''(P_*) - 2\alpha_u P_*^4\right)\phi \\ & - 3\alpha_u \left(1 - P_*^2\right) P_*^2 \frac{1}{2\pi} \int_0^{2\pi} \phi(\theta') d\theta'. \end{aligned}$$

Note the extra term linear in ϕ compared with Eq. S6 owing to the even parity of the constant base state rather than the odd parity of a cyclosis solution. The constant solution $\phi \equiv \phi_0$ has growth rate

$$\lambda_0 = -d^{(r)} + \alpha_p \left(1 - 3P_*^2\right) = -2\alpha_p P_*^2 < 0,$$

so this mode is always stable. The other solutions are of the form $\phi \propto e^{in\theta}$ for positive integer n , with growth rates

$$\begin{aligned} \lambda_n = & -d^{(s)}n^2 - \left[W''(P_*) - 2\alpha_u P_*^4\right] \\ = & -d^{(s)}n^2 - 2\alpha_p P_*^2 + 3\frac{\alpha_u}{\alpha_p} \left(1 - \frac{d^{(r)}}{\alpha_p}\right) d^{(r)}. \end{aligned}$$

From this, it is clear that the least stable mode is $n=1$. Fig. S2 shows the contour $\lambda_1=0$ as a function of (α_u, α_p) with $d^{(s)} = d^{(r)} = 0.025$. Although there is a region where the unidirectional solution is unstable, it is relatively slim, indicating that for the majority of parameter space there exists “bistability” in the system: both the cyclosis solution and the unidirectional solution can co-exist and be stable, so which one is selected depends upon their respective basins of attraction. We will now see that the basin of attraction for the unidirectional solution tends to shrink as α_u grows, leaving the cyclosis solution dominant for most initial conditions.

Basin of Attraction. We now know that both cyclosis and unidirectional solutions are usually stable. Because of this, the behavior of the system from given initial conditions becomes important. Indeed, as shown in the main text (Fig. 5), for smaller values of α_u the system can find both constant and cyclosis states depending on the initial configuration, necessitating multiple runs with different initial conditions to determine the typical behavior.

To understand this further, we will make explicit the competition between constant and cyclosis solutions by seeding the reduced model (Eq. S2) with initial conditions of purely $k=0$ and $k=1$ modes in Fourier space; we denote these mode amplitudes by \tilde{P}_0 and \tilde{P}_1 . Initial conditions with $\tilde{P}_1=0$ will always develop into the constant solution, and conversely $\tilde{P}_0=0$ will always develop cyclosis. Adjusting the ratio $\rho = \tilde{P}_1/\tilde{P}_0$ allows us to numerically map out the basin of attraction as model parameters vary by finding the critical crossover ρ_C separating initial conditions leading to constant and cyclosis solutions.

Fig. S3 illustrates numerically determined critical crossover curves $\rho_C(\alpha_p)$ for different values of α_u , with all other relevant parameters held fixed as in the main text. As α_u increases, it is easy to see that the critical region quickly becomes small, indicating that most random initial conditions will be attracted to the cyclosis state, as desired.

Pathologies

As discussed in the main text, it is possible to replicate certain pathologies and experimental streaming disruptions within our model by adjusting parameters appropriately.

In ref. 10, binding between the cell membrane and the cell wall is inhibited in *Vallisneria* mesophyll cells, causing actin cables to reorient from longitudinal to circumferential, encircling the long axis of the cell rather than running along it. Within our model, inhibiting binding corresponds to raising the restriction parameter ϵ and concomitantly lowering α_u , as filaments have fewer pinning points for polar reorientation to take effect. In addition, κ is likely to fall owing to the pliability and mobility of the filaments’ substrate giving less directionality and rigidity to any chemical or geometric directors.

With similar results, ref. 11 documents actin cable reorganization in *Lilium* pollen tubes by inhibiting microtubule polymerization. Actin cables then reorient circumferentially in the tip region where longitudinal microtubules are absent. The microtubules can be viewed as imposing a directionality on the actin; this is the origin of our repulsive direction \mathbf{d} with coupling constant κ . Depolymerizing the microtubules then corresponds to setting $\kappa \approx 0$, in the same fashion as the previous study.

Fig. S4 illustrates a simulation run showing the emergence of such a circumferential streaming pattern, with the parameter values used specified in the figure caption.

- Saintillan D, Shelley MJ (2008) Instabilities, pattern formation, and mixing in active suspensions. *Phys Fluids* 20(12):123304.
- Woodhouse FG, Goldstein RE (2012) Spontaneous circulation of confined active suspensions. *Phys Rev Lett* 109(16):168105.
- Jeffery GB (1922) The motion of ellipsoidal particles immersed in a viscous fluid. *Proc R Soc Lond A* 102(715):161–179.
- Doi M (1981) Molecular dynamics and rheological properties of concentrated solutions of rodlike polymers in isotropic and liquid crystalline phases. *J Polym Sci B Polym Phys* 19(2):229–243.
- Woodhouse FG, Goldstein RE (2012) Shear-driven circulation patterns in lipid membrane vesicles. *J Fluid Mech* 705:165–175.
- Batchelor GK (2000) *An Introduction to Fluid Dynamics* (Cambridge Univ Press, New York).
- Foissner I, Wastneys GO (2000) Microtubule disassembly enhances reversible cytochalasin-dependent disruption of actin bundles in characean internodes. *Protoplasma* 214(1–2):33–44.
- Pismen LM (2006) *Patterns and Interfaces in Dissipative Dynamics* (Springer, Berlin).
- Freitas P (1994) A nonlocal Sturm-Liouville eigenvalue problem. *Proc R Soc Edinburgh A* 124(1):169–188.
- Masuda Y, Takagi S, Nagai R (1991) Protease-sensitive anchoring of microfilament bundles provides tracks for cytoplasmic streaming in *Vallisneria*. *Protoplasma* 162(2–3):151–159.
- Foissner I, Grolig F, Obermeyer G (2002) Reversible protein phosphorylation regulates the dynamic organization of the pollen tube cytoskeleton: Effects of calyculin A and okadaic acid. *Protoplasma* 220(1–2):1–15.

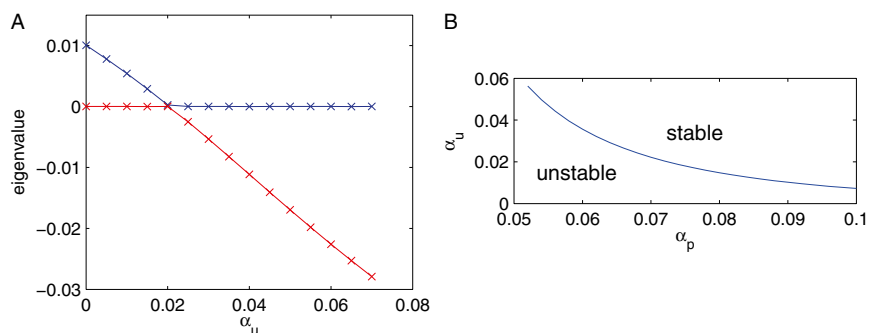


Fig. S1. (A) Sample trajectories of the two highest eigenvalues of the nonlocal problem (Eq. S6) as α_u varies, for $\alpha_p = 0.072$, with $d^{(s)} = d^{(r)} = 0.025$. The kink shows the eigenvalue crossover between instability and stability of cyclosis solutions. (B) Critical dividing line in (α_p, α_u) space between instability and stability of cyclosis solutions for long times, determined from eigenvalue trajectory crossovers as in A.

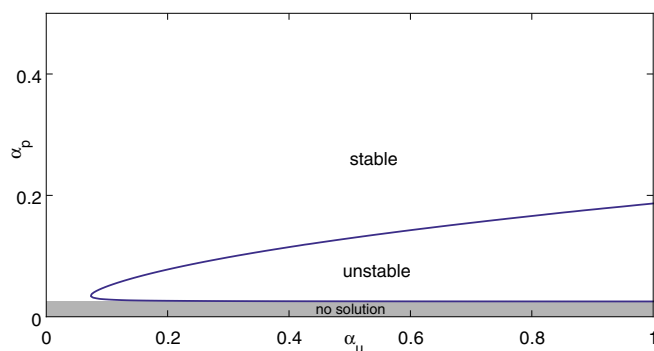


Fig. S2. Stability curve for the unidirectional solution in the (α_u, α_p) plane, for $d^{(s)} = d^{(r)} = 0.025$. The gray region denotes nonexistence of the base solution P_* .

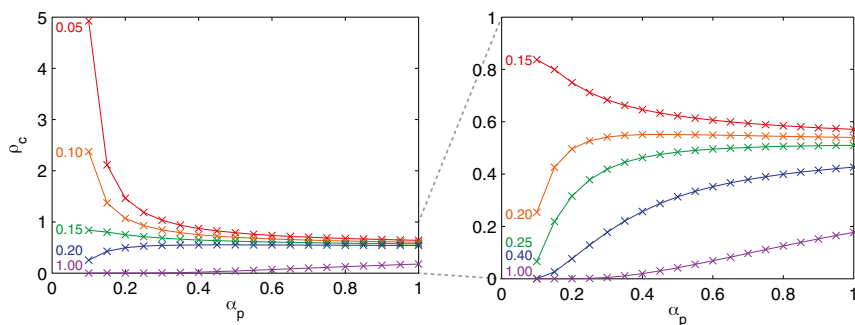


Fig. S3. Curves of $\rho_c(\alpha_p)$ dividing the basin of attraction between cyclosis and unidirectional solutions, for various values of α_u (indicated). The right-hand graph is an enlargement of the left with a shorter vertical scale.

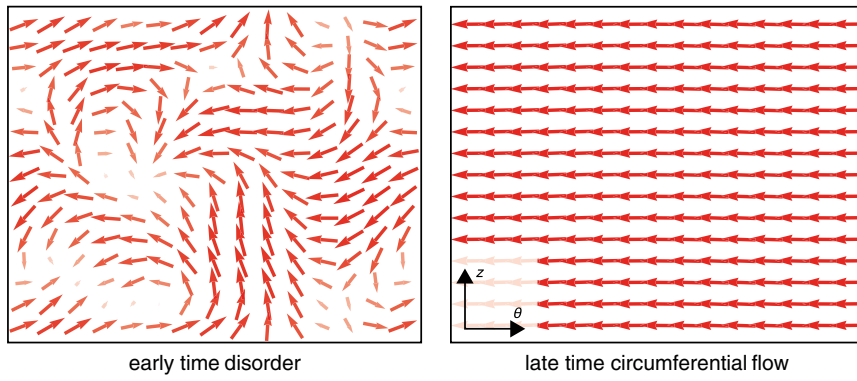


Fig. S4. Emergence of a circumferential streaming state on inhibition of repulsive directions and restriction. Parameters are $d^{(s)} = d^{(r)} = 0.025$, $\mu = 0.05$, $\epsilon = 0.8$, $\kappa = 0$, $\alpha_p = 0.8$, and $\alpha_u = 0.1$, with $\ell = 5$.